

# Quantum critical behaviour at the many-body localization transition

Matthew Rispoli<sup>1</sup>, Alexander Lukin<sup>1</sup>, Robert Schittko<sup>1</sup>, Sooshin Kim<sup>1</sup>, M. Eric Tai<sup>1</sup>, Julian Léonard<sup>1</sup> & Markus Greiner<sup>1\*</sup>

Phase transitions are driven by collective fluctuations of a system's constituents that emerge at a critical point<sup>1</sup>. This mechanism has been extensively explored for classical and quantum systems in equilibrium, whose critical behaviour is described by the general theory of phase transitions. Recently, however, fundamentally distinct phase transitions have been discovered for out-of-equilibrium quantum systems, which can exhibit critical behaviour that defies this description and is not well understood<sup>1</sup>. A paradigmatic example is the many-body localization (MBL) transition, which marks the breakdown of thermalization in an isolated quantum many-body system as its disorder increases beyond a critical value<sup>2–11</sup>. Characterizing quantum critical behaviour in an MBL system requires probing its entanglement over space and time<sup>4,5,7</sup>, which has proved experimentally challenging owing to stringent requirements on quantum state preparation and system isolation. Here we observe quantum critical behaviour at the MBL transition in a disordered Bose–Hubbard system and characterize its entanglement via its multi-point quantum correlations. We observe the emergence of strong correlations, accompanied by the onset of anomalous diffusive transport throughout the system, and verify their critical nature by measuring their dependence on the system size. The correlations extend to high orders in the quantum critical regime and appear to form via a sparse network of many-body resonances that spans the entire system<sup>12,13</sup>. Our results connect the macroscopic phenomenology of the transition to the system's microscopic structure of quantum correlations, and they provide an essential step towards understanding criticality and universality in non-equilibrium systems<sup>1,7,13</sup>.

The MBL transition<sup>8–11</sup> represents a type of quantum phase transition that fundamentally differs from both its classical and quantum ground-state counterparts<sup>2,3,7</sup>. Instead of being characterized by an instantaneous thermodynamic signature, it is identified by the system's inherent dynamic behaviour (Fig. 1a). In particular, the MBL transition manifests itself through a change in entanglement dynamics<sup>7,11</sup>. Recent years have seen tremendous progress in our understanding of both the thermal and the MBL phases within the frameworks of quantum thermalization<sup>6,14,15</sup> and emergent integrability<sup>4,5,8–11</sup>, respectively.

The quantum critical behaviour at this transition, however, has remained largely unresolved<sup>7</sup>. In particular, it is unclear whether the traditional association of collective fluctuations with static and dynamic critical behaviour can be applied to this transition. The high amount of entanglement found at the MBL transition limits numerical studies owing to the required computational power<sup>16,17</sup>. Several theoretical approaches, despite using disparate microscopic structures, suggest that anomalous transport is the macroscopic behaviour at the quantum critical point<sup>12,18–20</sup>. Experimental studies do indeed indicate a slowdown of the dynamics at intermediate disorder<sup>21,22</sup>. However, identifying anomalous transport as quantum critical dynamics is experimentally challenging, since similar behaviour can also originate from stochastic effects such as inhomogeneities in the initial state<sup>23</sup> or coupling to a

classical bath<sup>24,25</sup>. Additionally, in the case of random disorder, the presence of rare regions, where potential offsets accidentally coincide for consecutive lattice sites, permits several microscopic mechanisms that may govern this critical behaviour and therefore makes it challenging to distinguish between them<sup>26–28</sup>. Our experimental protocol overcomes these challenges by using a quasi-periodic potential, which is free of rare regions, as well as by evolving a pure, homogeneous initial state under unitary dynamics. Using this protocol, we observe quantum critical dynamics via anomalous transport, enhanced quantum fluctuations, and system-size-dependent thermalization. In addition, we microscopically resolve and characterize the structure of the entanglement in the many-body states through their multi-particle quantum correlations.

Our experiments start with a pure state of up to twelve unentangled lattice sites at unity filling (Fig. 1b). We study its out-of-equilibrium evolution after a rapid increase of the tunnelling in the bosonic, interacting Aubry–André Hamiltonian:

$$\hat{\mathcal{H}} = -J \sum_i (\hat{a}_i^\dagger \hat{a}_{i+1} + \text{H.c.}) + \frac{U}{2} \sum_i \hat{n}_i (\hat{n}_i - 1) + W \sum_i h_i \hat{n}_i$$

where  $\hat{a}_i^\dagger$  ( $\hat{a}_i$ ) is the creation (annihilation) operator for a boson on site  $i$ , and  $\hat{n}_i$  is the corresponding particle number operator (H.c. is the Hermitian conjugate). The tunnelling time  $\tau = \hbar/J = 4.3(1)$  ms (with the reduced Planck constant  $\hbar$ ) between neighbouring sites and the pairwise interaction energy  $U = 2.87(3)J$  remain constant for all experiments. The potential energy offset  $h_i = \cos(2\pi\beta i + \phi)$  on site  $i$  follows a quasi-periodic distribution of amplitude  $W$ , period  $1/\beta \approx 1.618$  lattice sites and phase  $\phi$ . After a variable evolution time, we obtain full counting statistics of the quantum state through a fluorescence imaging technique. The applied unitary evolution preserves the initial purity of 99.1(2)% per site, such that all correlations are expected to stem from entanglement in the system<sup>11,15</sup>.

We first characterize the system's dynamical behaviour by studying its transport properties for different disorder strengths. Since the initial state has exactly one atom per site, the system starts with zero density correlations at all length scales. However, during the Hamiltonian evolution, tunnelling dynamics build up anti-correlated density fluctuations between coupled sites of increasing distance (Fig. 2a). Motivated by this picture, we quantify the particle dynamics by defining the transport distance,  $\Delta x \propto \sum_d d \times \langle G_c^{(2)}(i, i+d) \rangle$ , as the first moment of the disorder-averaged two-point density correlations,  $G_c^{(2)}(i, i+d) = \langle \hat{n}_i \hat{n}_{i+d} \rangle - \langle \hat{n}_i \rangle \langle \hat{n}_{i+d} \rangle$  (Supplementary Information section 7). At low disorder, we observe these anti-correlations to rapidly build up and saturate over a timescale of  $t/\tau \approx L/2$ . With increasing disorder, we observe a slowdown of particle transport that is consistent with a power-law growth  $\Delta x \propto t^\alpha$  (Fig. 2b)<sup>29</sup>. We extract the anomalous diffusion exponent  $\alpha$  from a subset of the data points that exclude the initial transient dynamics in the system ( $L/2 < t/\tau \leq 100$ ) (inset to Fig. 2b). The exponent  $\alpha$  is reduced by successively higher disorder, demonstrating the suppression of transport in the MBL regime.

<sup>1</sup>Department of Physics, Harvard University, Cambridge, MA, USA. \*e-mail: greiner@physics.harvard.edu

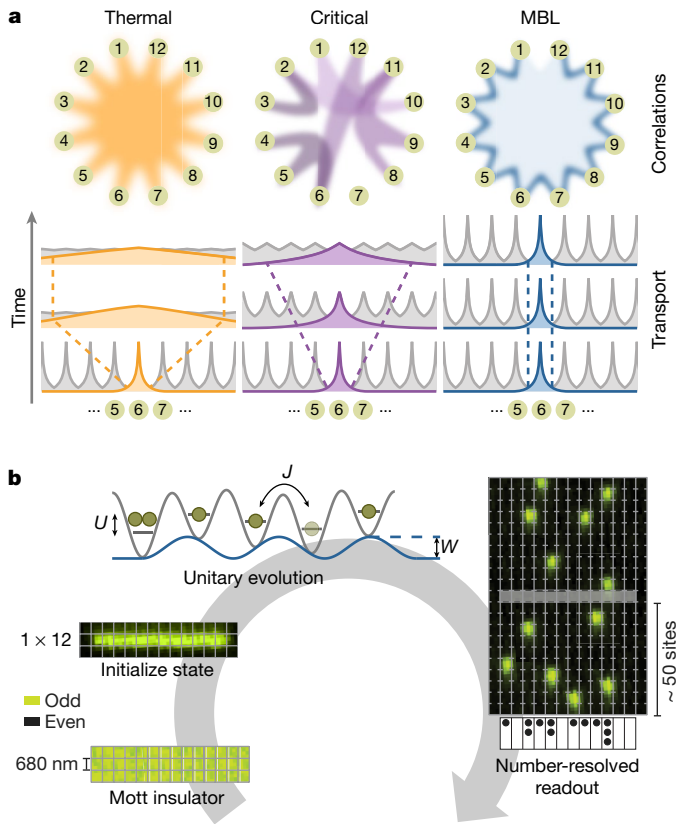


**Fig. 1 | Microscopy of the many-body localization transition.**

**a**, Illustration of the quantum correlations among the lattice sites after a long evolution time in the presence of weak (thermal), intermediate (critical) and strong disorder (MBL). In the critical regime, a complex pattern of multi-particle correlations spans all length scales. This pattern is visualized by shaded links between different lattice sites. In contrast, the thermal and MBL regimes exhibit uniformly distributed and predominantly local correlations, respectively. These correlations occur in conjunction with a change in transport properties, which transition from diffusive (thermal) to anomalous (critical) to vanishing (MBL), as depicted by the evolution of an initially localized test charge (coloured) within a homogeneous system (grey). **b**, We initialize the system as a pure product state of up to twelve lattice sites at unity filling. The system becomes entangled under the unitary, non-equilibrium dynamics of the bosonic, interacting Aubry–André model with on-site interaction energy  $U$ , particle tunnelling at rate  $J/\hbar$ , and quasi-periodic potential with amplitude  $W$ . After a variable evolution time, we measure the atom number on each lattice site through a fluorescence imaging technique (Supplementary Information section 1).

To identify the anomalous diffusion as a signature of quantum critical dynamics, we measure the system-size dependence of two observables in the long-time limit ( $t = 100\tau$ ): the on-site number fluctuations  $\mathcal{F} \equiv G_c^{(2)}(d=0)$  as a probe of local thermalization, and the transport distance  $\Delta x$  as a localization measure (Fig. 2c). At low disorder, the fluctuations agree with those predicted by a thermal ensemble and particles are completely delocalized for both system sizes. This demonstrates that local quantum thermalization occurs independently of system size at low disorder and establishes that this regime corresponds to the system being in the thermal phase. At strong disorder, the physics is governed by the formation of an intrinsic length scale, namely the localization length  $\xi \approx \Delta \bar{x}$  (refs<sup>10,11</sup>). We observe system-size-independent, sub-thermal fluctuations and measure an intrinsic length scale  $\Delta \bar{x}$ . This indicates that the strong disorder regime corresponds to the system being in the localized phase. However, at intermediate disorder, we observe

that our data are consistent with a theoretically predicted system-size dependence for both observables. This suggests the absence of an intrinsic length scale and the presence of finite-size-limited fluctuations, which identify the critically thermalizing regime (Supplementary Information section 4). These measurements of system-size-dependent thermalization can be visualized as two horizontal cuts in a finite-size phase diagram. The observed finite-size dependence is consistent with the physics associated with a critically thermalizing intermediate phase and a shrinking quantum critical cone (inset to Fig. 2c)<sup>1</sup>.

We then investigate the multi-particle correlations in the system to probe the presence of enhanced quantum fluctuations in the quantum critical regime. For this study, we employ the  $n$ -point connected density-correlation functions (Fig. 2d)<sup>30–32</sup>:

$$G_c^{(n)}(x) = G_{\text{tot}}^{(n)}(x) - G_{\text{dis}}^{(n)}(x)$$

which act on lattice sites with positions  $x = (x_1, \dots, x_n)$ . The disconnected part of this function,  $G_{\text{dis}}^{(n)}$ , is fully determined by all lower-order correlation functions, and therefore does not contain new information at order  $n$ . By removing it from the total measured correlation function,  $G_{\text{tot}}^{(n)}(x) = \langle \prod_{k=1}^n \hat{n}(x_k) \rangle$ , we isolate all  $n$ -order correlations that are independent of lower-order processes (Supplementary Information sections 2, 3). This approach gives a direct handle on the level of complexity of the underlying many-body wavefunction and characterizes its entanglement via its non-separability into subsystems of size smaller than  $n$ . We quantify the relevance of order  $n$  processes by computing the mean absolute value of all correlations arising from both contiguous and non-contiguous  $n$  sites in the system (Fig. 2e). We find that in the thermal and the many-body-localized regimes, the system becomes successively less correlated at higher order. The behaviour in the quantum critical regime is strikingly different: we observe that the system is strongly correlated at all measured orders.

To reveal the microscopic origin for the anomalous transport, we now investigate the site-resolved structure of the many-body state (Fig. 3a). We first study how much each lattice site contributes to the transport by considering the site-resolved two-point correlations in the long-time limit ( $t = 100\tau$ ). In the thermal regime, we find similar correlations between all lattice sites, which correspond to uniformly delocalized atoms. In contrast, density correlations are restricted to nearby sites in the MBL regime owing to localization. At intermediate disorder, we observe strongly inhomogeneous correlations, revealing a sparse structure that involves only specific distances between lattice sites, yet spans the entire system size.

The sparse structure is expected to be linked to the applied quasi-periodic potential. The average energy offsets of sites  $d$  apart in the system are correlated by this potential. This correlation is then inherited by the system's fluctuations when the interaction energy  $U$  compensates for these correlated offsets. To investigate this structure, we compare the two-point density correlations with the autocorrelation function,  $A(d) = \langle h_i h_{i+d} \rangle_i$ , of the quasi-periodic potential. Indeed, we find that the site-averaged connected density correlations  $G_c^{(2)}(d) = \langle G^{(2)}(i, i+d) \rangle_i$  inherit their spatial structure from  $A(d)$  (Fig. 3b). We find that this contribution is maximal in the critical regime but is strongly reduced in the thermal and MBL regimes (Fig. 3c). These observations contrast with the behaviour of a non-interacting system, where the sign of the structure is opposite because resonant tunnelling is favoured for zero potential energy difference. These results illustrate microscopically how the interplay of strong interactions and disorder can lead to anomalous diffusion. However, this picture of effective single-particle hopping that couples distant sites neglects the many-body nature of these systems.

To investigate the system's many-body structure, we examine the site-resolved contributions of the three-point correlations. Since all non-zero contributions to the three-point correlations involve

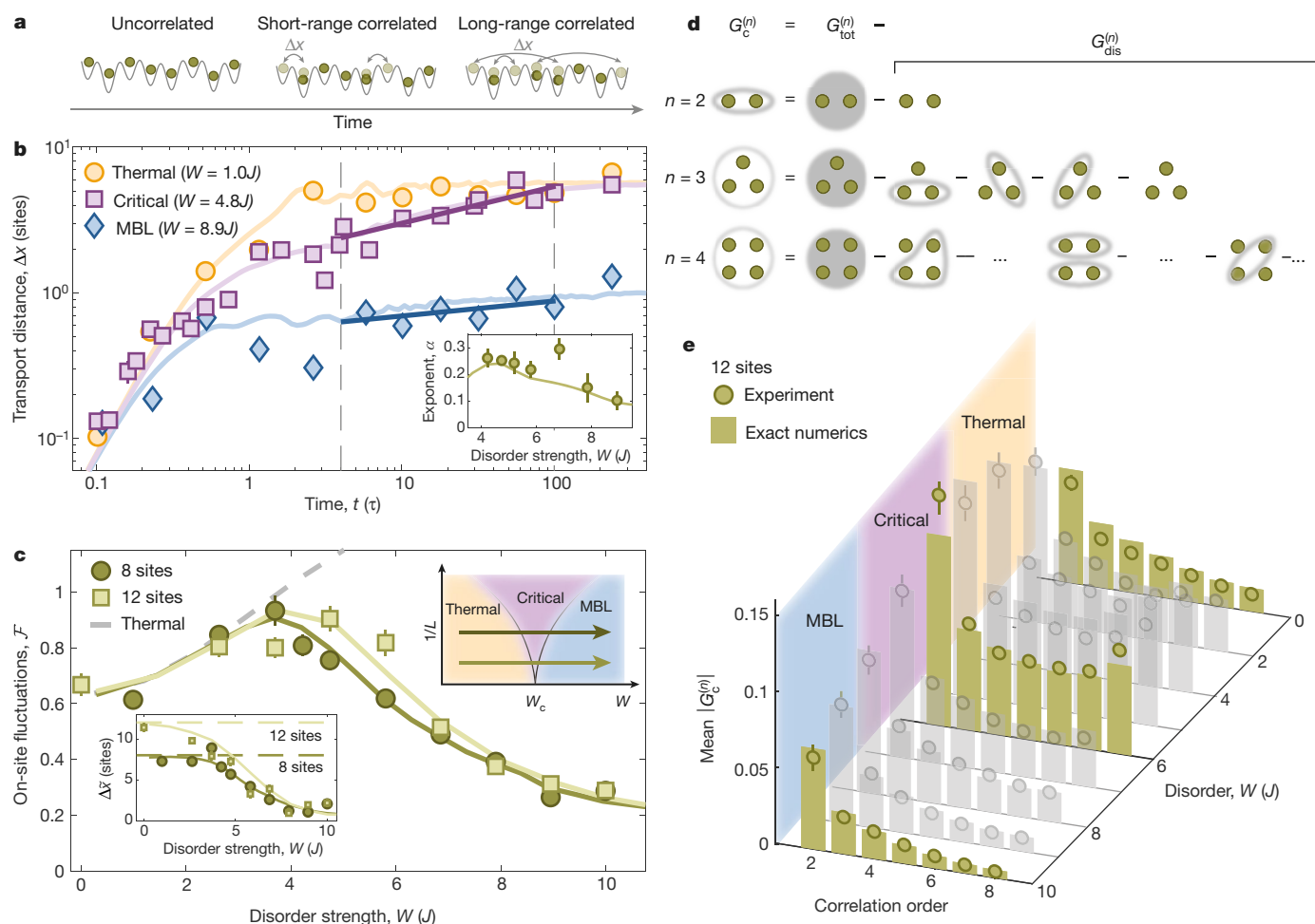


**Fig. 2 | Quantum critical dynamics at the MBL transition.** **a**, The initially uncorrelated system develops two-point density correlations under its transport dynamics. Short-range correlations emerge within one tunnelling time  $\tau = \hbar/J$ , whereas the diffusion exponent  $\alpha$  determines the timescale over which correlations form across the system size  $L$ . **b**, Particle transport, characterized by the transport distance (measured in lattice sites), slows down at intermediate disorder, consistent with a power-law evolution with exponent  $\alpha < 0.5$ , demonstrating subdiffusive dynamics (inset). These data were taken on an eight-site system. **c**, The critical nature of the dynamics is determined from the behaviour of on-site density fluctuations  $\mathcal{F}$  and the transport distance  $\Delta\bar{x}$  (lower left inset) at long times ( $t = 100\tau$ ) for both system sizes considered. The thermal regime is determined by the agreement of the measured  $\mathcal{F}$  with the prediction from a thermal ensemble (dashed grey line). The system-size

correlated hopping of at least two particles, they are a signature for multi-particle entanglement<sup>31</sup>. In the quantum critical regime, we find that these correlations span the entire system and are highly structured, taking on both positive and negative values (Fig. 4a). In contrast to the pattern in the second-order correlation function, this third-order structure is not directly recognizable as the quasi-periodic-potential correlations. To gain further insight into the structure, we analyse the contributions of all possible particle configurations in Fig. 4b. In particular, for  $G_c^{(3)}(d_1 = 3, d_2 = 1)$  which is positive, we see that the dominant contribution comes from a particular process that favours multiple atoms hopping to the same site. In contrast,  $G_c^{(3)}(d_1 = 3, d_2 = 2)$ , which is negative, has a dominant process that favours all atoms leaving the three sites considered. Although this provides some intuition for the emergent many-body resonances, the three-point correlations are, in fact, the result of a superposition of many correlated processes. These observations further demonstrate how the interactions between multiple atoms can compensate for the disorder via correlated tunneling of several atoms. In this way, we can

see the additional part that interactions play in the disordered system: they supply higher-order many-body resonances that preserve transport where lower-order processes are energetically suppressed. Our results demonstrate how a many-body, sparse resonant structure drives the quantum critical behaviour at the MBL transition. This observed microscopic description is consistent with the theoretically suggested mechanisms of a sparse backbone of resonances that can act as a functional bath for the system<sup>12,13,33</sup>. However, our results provide a new perspective on this description by mapping out the prevalence of high-order processes in the system that facilitate this critical thermalization. In future experiments, the tunability of our system will allow us to address further open questions on the MBL transition, such as possible discontinuities of the entanglement entropy<sup>13</sup>, the potential emergence of new dynamic phases near the critical point, and the influence of rare regions in the disorder potential<sup>26,27</sup>. Furthermore, the demonstrated techniques pave the way to exploring the role of universality in non-equilibrium systems. From a computational perspective, our

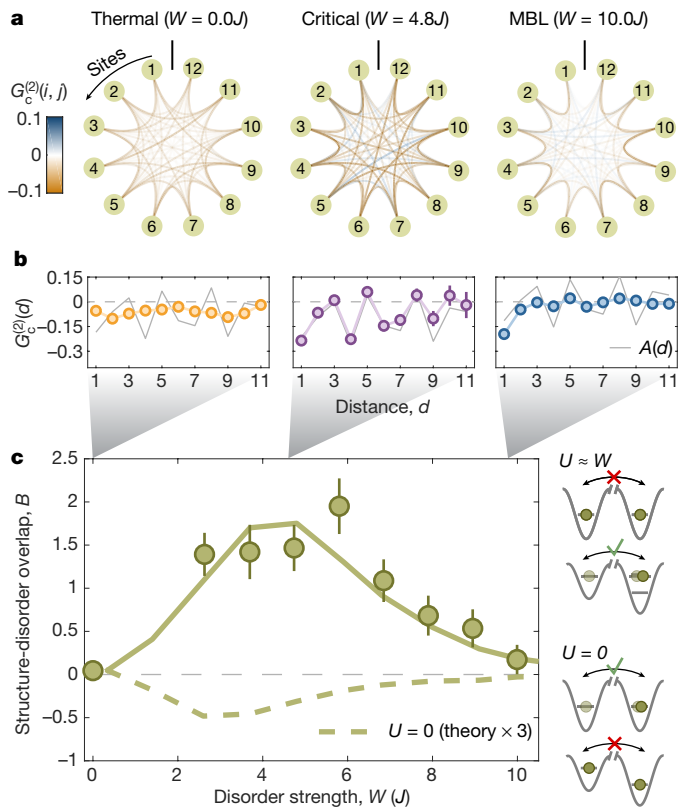


**Fig. 3 | Sparse network of resonances.** **a**, The measured site-dependent two-point correlations  $G_c^{(2)}(i, j)$  are plotted for all inter-site combinations, whose amplitudes are represented by the coloured lines connecting the lattice sites  $i$  and  $j$ . In the quantum critical regime, correlations preferably form at specific distances, showing a network-like structure. This contrasts with homogeneous correlations in the thermal regime and nearest-neighbour correlations in the MBL regime. **b**, The structure of the correlation network is revealed by the averaged correlation function  $G_c^{(2)}(d) = \langle G_c^{(2)}(i, i+d) \rangle_i$ . Its similarity to the autocorrelation  $A(d) = \langle h_i h_{i+d} \rangle_i$  of the quasi-periodic potential (solid grey line) indicates interaction-induced tunnelling processes that are enhanced when the interaction energy compensates for the potential energy difference. **c**, We quantify the similarity by the overlap  $B \propto \sum_{d=2}^L G_c^{(2)}(d)A(d)$  across all inter-site distances  $d > 1$  (Supplementary Information sections 7, 8), which is maximal in the quantum critical regime. The sign of the overlap would be opposite for non-interacting particles (dashed line), which favours tunnelling between sites with similar potential energies. The solid lines in **b**, **c** and the dashed line in **c** denote the prediction of exact numeric time evolution calculations without any free parameters (Supplementary Information section 5). The error bars are the s.e.m. (Supplementary Information section 9).

system's Hilbert space dimension is comparable to the dimension of 22 spins with zero total magnetization. A moderate increase of the system's spatial dimension beyond this experiment results in numerically intractable sizes.

**Data availability**

The data that support the findings of this study are available in the Dataverse repository at <https://doi.org/10.7910/DVN/E2ROXU>.

**Online content**

Any methods, additional references, Nature Research reporting summaries, source data, extended data, supplementary information, acknowledgements, peer review information; details of author contributions and competing interests; and statements of data and code availability are available at <https://doi.org/10.1038/s41586-019-1527-2>.

Received: 16 December 2018; Accepted: 3 July 2019; Published online 4 September 2019.

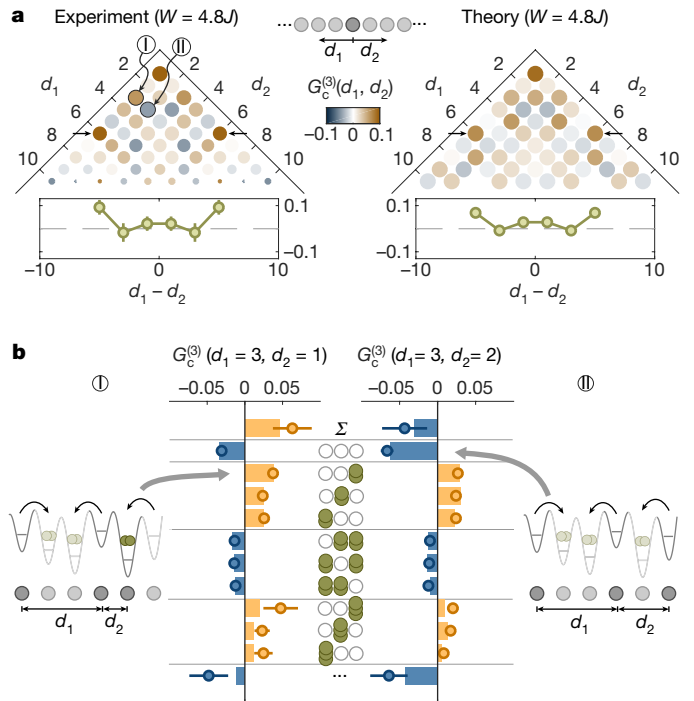


**Fig. 4 | Many-body correlations in the quantum critical regime.** **a**, The connected correlation function (unitless),  $G_c^{(3)}(d_1, d_2)$ , for three lattice sites spaced by distances  $d_1$  and  $d_2$  in the quantum critical regime ( $W = 4.8J$ ,  $t = 100\tau$ ), showing the strongly interacting nature of the state. We find that the three-point correlations show a characteristic structure that is governed by the contribution of the number states on the considered sites. The arrows indicate the cut in  $d_1, d_2$  space plotted below. **b**, To exemplify the relevant processes of order  $n = 3$ , we show the contributions of the number states on lattice sites at distance  $d_1 = 3, d_2 = 1$  (left, circled I) and  $d_1 = 3, d_2 = 2$  (right, circled II). Although there is a wide distribution of contributing configurations, the relative dominance of a particular process provides the overall structure in **a**. The illustration of atoms undergoing a highly correlated hopping process in the lattice describes how such correlations can contribute to either positive or negative correlations among the three considered sites. The theory plot in **a** and bars in **b** are calculated from exact numeric time calculations without any free parameters. The inverse marker size in the experimental plot in **a** and the error bars in both **a** and **b** denote the s.e.m. (Supplementary Information section 9).

1. Täuber, U. C. Phase transitions and scaling in systems far from equilibrium. *Annu. Rev. Condens. Matter Phys.* **8**, 185–210 (2017).
2. Basko, D. M., Aleiner, I. L. & Altshuler, B. L. On the problem of many-body localization. *Ann. Phys.* **321**, 1126 (2006).
3. Pal, A. & Huse, D. A. Many-body localization phase transition. *Phys. Rev. B* **82**, 174411 (2010).
4. Serbyn, M., Papic, Z. & Abanin, D. A. Local conservation laws and the structure of the many-body localized states. *Phys. Rev. Lett.* **111**, 127201 (2013).
5. Huse, D. A., Nandkishore, R. & Oganesyan, V. Phenomenology of fully many-body-localized systems. *Phys. Rev. B* **90**, 174202 (2014).
6. D'Alessio, L., Kafri, Y., Polkovnikov, A. & Rigol, M. From quantum chaos and eigenstate thermalization to statistical mechanics and thermodynamics. *Adv. Phys.* **65**, 239–362 (2016).
7. Abanin, D. A., Altman, E., Bloch, I. & Serbyn, M. Ergodicity, entanglement and many-body localization. Preprint at <https://arxiv.org/abs/1804.11065> (2018).
8. Schreiber, M. et al. Observation of many-body localization of interacting fermions in a quasirandom optical lattice. *Science* **349**, 842–845 (2015).
9. Smith, J. et al. Many-body localization in a quantum simulator with programmable random disorder. *Nat. Phys.* **12**, 907–911 (2016).
10. Choi, J. et al. Exploring the many-body localization transition in two dimensions. *Science* **352**, 1547–1552 (2016).
11. Lukin, A. et al. Probing entanglement in a many-body-localized system. *Science* **364**, 256–260 (2019).
12. Potter, A. C., Vasseur, R. & Parameswaran, S. A. Universal properties of many-body delocalization transitions. *Phys. Rev. X* **5**, 031033 (2015).
13. Khemani, V., Lim, S. P., Sheng, D. N. & Huse, D. A. Critical properties of the many-body localization transition. *Phys. Rev. X* **7**, 021013 (2017).
14. Neill, C. et al. Ergodic dynamics and thermalization in an isolated quantum system. *Nat. Phys.* **12**, 1037–1041 (2016).

15. Kaufman, A. M. et al. Quantum thermalization through entanglement in an isolated many-body system. *Science* **353**, 794–800 (2016).
16. Agarwal, K., Gopalakrishnan, S., Knap, M., Müller, M. & Demler, E. Anomalous diffusion and Griffiths effects near the many-body localization transition. *Phys. Rev. Lett.* **114**, 160401 (2015).
17. Setiawan, F., Dong, L. D. & Pixley, J. H. Transport properties across the many-body localization transition in quasiperiodic and random systems. *Phys. Rev. B* **96**, 104205 (2017).
18. Vosk, R., Huse, D. A. & Altman, E. Theory of the many-body localization transition in one-dimensional systems. *Phys. Rev. X* **5**, 031032 (2015).
19. Dumitrescu, P. T., Vasseur, R. & Potter, A. C. Scaling theory of entanglement at the many-body localization transition. *Phys. Rev. Lett.* **119**, 110604 (2017).
20. Goremykina, A., Vasseur, R. & Serbyn, M. Analytically solvable renormalization group for the many-body localization transition. Preprint at <https://arxiv.org/abs/1807.04285> (2018).
21. Lüschen, H. P. et al. Observation of slow dynamics near the many-body localization transition in one-dimensional quasiperiodic systems. *Phys. Rev. Lett.* **119**, 260401 (2017).
22. Bordia, P. et al. Probing slow relaxation and many-body localization in two-dimensional quasiperiodic systems. *Phys. Rev. X* **7**, 041047 (2017).
23. Luitz, D. J., Laflorencie, N. & Alet, F. Extended slow dynamical regime close to the many-body localization transition. *Phys. Rev. B* **93**, 060201 (2016).
24. Nandkishore, R., Gopalakrishnan, S. & Huse, D. A. Spectral features of a many-body-localized system weakly coupled to a bath. *Phys. Rev. B* **90**, 064203 (2014).
25. Lüschen, H. P. et al. Signatures of many-body localization in a controlled open quantum system. *Phys. Rev. X* **7**, 011034 (2017).
26. De Roeck, W. & Huveneers, F. Stability and instability towards delocalization in many-body localization systems. *Phys. Rev. B* **95**, 155129 (2017).
27. Nandkishore, R. & Gopalakrishnan, S. Many body localized systems weakly coupled to baths. *Ann. Phys.* **529**, 1600181 (2017).
28. Agarwal, K. et al. Rare-region effects and dynamics near the many-body localization transition. *Ann. Phys.* **529**, 1600326 (2017).
29. Lucioni, E. et al. Observation of subdiffusion in a disordered interacting system. *Phys. Rev. Lett.* **106**, 230403 (2011).
30. Liu, H.-C. High-order correlation of chaotic bosons and fermions. *Phys. Rev. A* **94**, 023827 (2016).
31. Schweigler, T. et al. Experimental characterization of a many-body system via higher-order correlations. *Nature* **545**, 323–326 (2017).
32. Hodgman, S. S., Khakimov, R. I., Truscott, A. G. & Kheruntsyan, K. V. Solving the quantum many-body problem via correlations measured with a momentum microscope. *Phys. Rev. Lett.* **118**, 240402 (2017).
33. Grover, T. Certain general constraints on the many-body localization transition. Preprint at <https://arxiv.org/abs/1405.1471> (2014).

**Publisher's note:** Springer Nature remains neutral with regard to jurisdictional claims in published maps and institutional affiliations.

© The Author(s), under exclusive licence to Springer Nature Limited 2019

**Acknowledgements** We acknowledge discussions with D. Abanin, E. Altman, H. Bernien, C. Chiu, S. Choi, E. Demler, A. Hébert, W. W. Ho, V. Kasper, V. Khemani, J. Kwan, L. Santos and J. Schmiedmayer. We were supported by grants from the National Science Foundation, the Gordon and Betty Moore Foundations EPIQS Initiative, an Air Force Office of Scientific Research MURI programme, an Army Research Office MURI programme and the NSF Graduate Research Fellowship Program. J.L. acknowledges support from the Swiss National Science Foundation.

**Author contributions** All authors contributed extensively to the construction of the experiment, the collection and analysis of the data, and the writing of the manuscript. M.G. supervised the work.

**Competing interests** The authors declare no competing interests.

**Additional information**

**Supplementary information** is available for this paper at <https://doi.org/10.1038/s41586-019-1527-2>.

**Correspondence and requests for materials** should be addressed to M.G.

**Peer review information** *Nature* thanks Maksym Serbyn and Jean-Philippe Brantut for their contribution to the peer review of this work.

**Reprints and permissions information** is available at <http://www.nature.com/reprints>.